The Sumatra subduction zone: A case for a locked fault zone extending into the mantle

Martine Simoes[1]
Laboratoire de Geologie, Ecole Normale Supérieure, Paris, France

Jean Philippe Avouac
Geology and Planetary Sciences Division, California Institute of Technology, Pasadena, California, USA

Rodolphe Cattin and Pierre Henry[2]
Laboratoire de Geologie, Ecole Normale Supérieure, Paris, France

Received 23 December 2003; revised 28 June 2004; accepted 26 July 2004; published 2 October 2004.

[1] A current view is that the portion of the subduction interface that remains locked in the time interval between large interplate earthquakes, hereinafter referred to as the locked fault zone (LFZ), does not extend into the mantle because serpentinization of the mantle wedge would favor stable aseismic sliding. Here, we test this view in the case of the Sumatra subduction zone where the downdip end of the LFZ can be well constrained from the pattern and rate of uplift deduced from coral growth and from GPS measurements of horizontal deformation. These geodetic data are modeled from a creeping dislocation embedded in an elastic half-space and indicate that the LFZ extends 132 ± 10/7 km from the trench, to a depth between 35 and 57 km. By combining this information with the geometry of the plate interface as constrained from two-dimensional gravimetric modeling and seismicity, we show that the LFZ extends below the forearc Moho, which is estimated to lie at a depth of ~30 km, at a horizontal distance of 110 km from the trench. So, in this particular island arc setting, the LFZ most probably extends into the mantle, implying that either the mantle is not serpentinized, or that the presence of serpentine does not necessarily imply stable sliding. From thermal modeling, the temperature at the downdip end of the LFZ is estimated to be 260 ± 100°C. This temperature seems too low for thermally activated ductile flow, so that aseismic slip is most probably due to pressure and/or temperature induced steady state brittle sliding, possibly favored by fluids released from the subducting slab. *INDEX TERMS:* 7223 Seismology: Seismic hazard assessment and prediction; 1206 Geodesy and Gravity: Crustal movements—interplate (8155); 1219 Geodesy and Gravity: Local gravity anomalies and crustal structure; 3902 Mineral Physics: Creep and deformation; *KEYWORDS:* locked fault zone, interseismic deformation, Sumatra

Citation: Simoes, M., J. P. Avouac, R. Cattin, and P. Henry (2004), The Sumatra subduction zone: A case for a locked fault zone extending into the mantle, *J. Geophys. Res.*, *109*, B10402, doi:10.1029/2003JB002958.

1. Introduction

[2] Major subduction thrust earthquakes are generated over a limited depth range, generally between 20 and 70 km [*Pacheco et al.*, 1993; *Tichelaar and Ruff*, 1993], rupturing the portion of the plate interface referred here as the "seismogenic zone." These main interplate events are thought to nucleate within the portion of the plate interface that remains fully or partially locked in the time interval between large earthquakes (Figure 1) and to rupture this portion fully or partially; they might also extend deeper due to the dynamics of the rupture process [e.g., *Scholz*, 1998] (Figure 1). Assessing the width and degree of locking of the locked fault zone (hereinafter referred to as LFZ) is therefore of uppermost importance for assessing seismic hazard along subduction zones. This information can be deduced from geodetic measurements of interseismic strain [*Oleskevich et al.*, 1999]. Uplift data are particularly critical to this respect, since the maximum uplift rate can be taken as a good indicator of the horizontal position of the downdip end of the LFZ (Figure 1). A better understanding of the physical factors governing these characteristics would thus be most useful.

[3] The downdip end of the LFZ is thought to correspond to the transition from slip-weakening friction to aseismic

[1] Also at Geology and Planetary Sciences Division, California Institute of Technology, Pasadena, California, USA.

[2] Now at Centre Européen de Recherche et d'Enseignement de Géosciences de l'Environnement, College de France, Aix-en-Provence, France.

0148-0227/04/2003JB002958$09.00

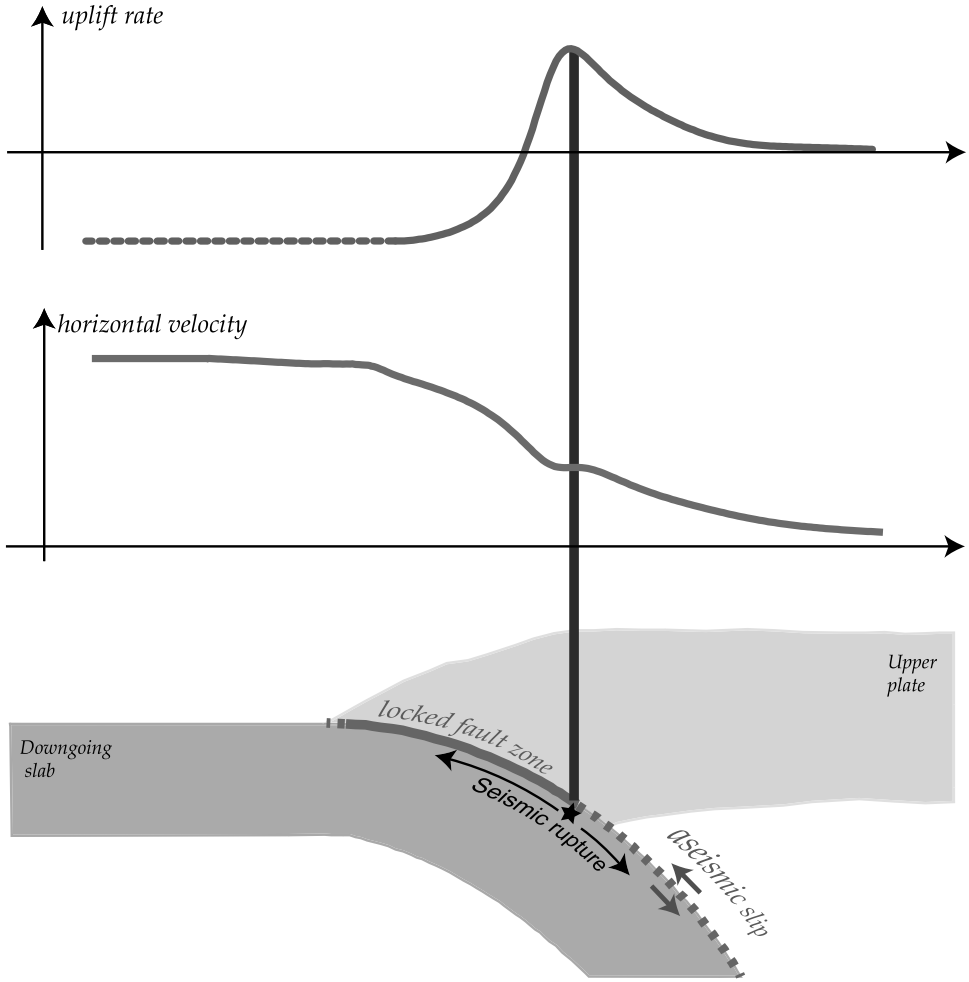

Figure 1. Diagram showing how the geometry of the locked fault zone (LFZ) relates to the pattern of uplift and horizontal velocities (relative to the upper plate far from the trench). The zone of maximum vertical uplift lies more or less above the transition to aseismic slip at depth (actually this relationship also depends on the dip angle of the plate interface at this location); therefore vertical data put tighter constraints on the location of the downdip end of the LFZ than does the horizontal deformation. Major earthquakes are thought to nucleate along the LFZ, but rupture might propagate downdip into the aseismic sliding portion of the plate interface. For simplicity, no transition zone between the fully locked portion of the fault and the zone of aseismic slip at depth was represented on this diagram. It might be recalled that the back slip dislocation used to invert the interseismic data does not need to match the actual geometry of the LFZ: it only needs to be tangent to the plate interface at the transition from seismic to aseismic slip at the downdip end of the LFZ [*Dragert et al.*, 1994; *Vergne et al.*, 2001].

stable sliding [*Hyndman et al.*, 1997]. According to laboratory experiments and field observations, this thermally activated transition occurs at a temperature around 325–350°C for quartzo-feldspathic rocks [*Blanpied et al.*, 1991, 1995], and around 750°C for unaltered mantle rocks [*Bergman and Solomon*, 1988; *Wiens and Stein*, 1983]. This is in keeping with the observation that the downdip extent of the LFZ generally coincides with the 350°C isotherm if this temperature is reached above the Moho [*Oleskevich et al.*, 1999]. However, in the case of a thinner forearc crust or colder subducting slab, it is generally observed that the transition occurs where the thrust fault intersects the forearc Moho, possibly because the systematic presence of serpentinite or other hydrated minerals in the mantle wedge would allow aseismic slip along the plate interface [*Peacock and Hyndman*, 1999]. However, it has been reported that at some places, the LFZ might extend into the mantle. This may hold for the Japan Trench since the forearc Moho is ~20–25 km deep [*Hayakawa et al.*, 2002; *Miura et al.*, 2003, 2001; *Takahashi et al.*, 2000] and the LFZ extends to depths of 50–55 km [*Mazzotti et al.*, 2000]. It could also be the case in certain island arc settings such as the eastern Aleutians where the forearc crust is presumably 20 km thick at the plate interface [*Holbrook et al.*, 1999; *Lizarralde et al.*, 2002] while the LFZ might extend deeper since thrust events are generated to depths of 35–40 km [*Tichelaar and*

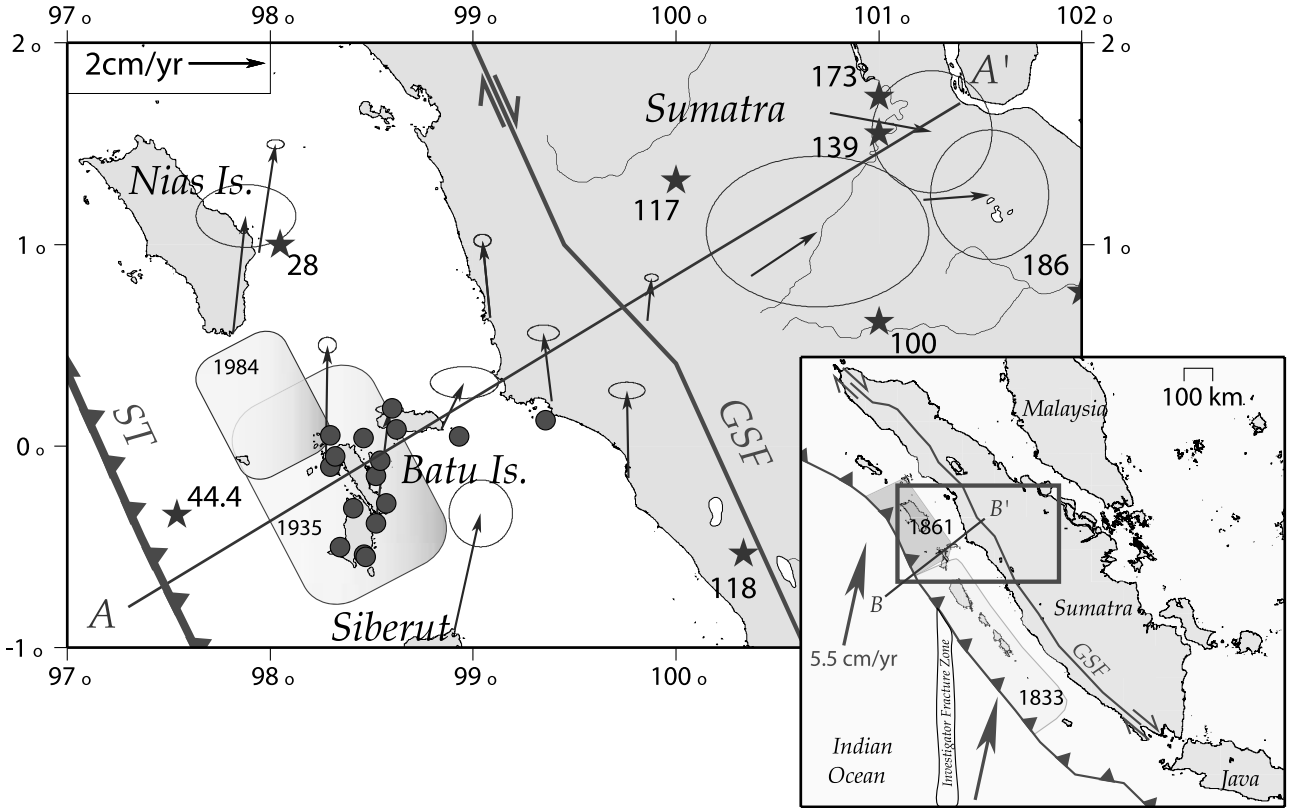

Figure 2. Location of study area. Circles indicate that location of coral data is from *Natawidjaja et al.* [2004]. Arrows indicate GPS horizontal velocities relative to Sunda Shelf [*Bock et al.*, 2003] with ellipse errors at the 95% confidence level. Stars indicate heat flow data with their values in mW m^{-2} [*Pollack et al.*, 1993; *Vacquier and Taylor*, 1966]. Estimated plane ruptures for the 1935 and 1984 earthquakes were reported within their uncertainties [*Rivera et al.*, 2002]. Interseismic straining data were projected on the A-A′ cross section (Figure 3). The Sumatran Trench (ST) and the Great Sumatran Fault (GSF) are also indicated. The volcanic arc lies approximately along this latter major fault. Insert shows geodynamical context with the Australia-Sunda Shelf convergence velocity of *Bock et al.* [2003]; line B-B′ locates the gravimetric profile. Probable plane ruptures of the 1833 ($M \sim 9$) and 1861 ($M \sim 8.5$) subduction earthquakes are reported [*Newcomb and McCann*, 1987]. The Investigator Fracture Zone is also indicated.

Ruff, 1993]. This may also be true along the Sumatra subduction zone. Indeed, previous studies of the pattern of interseismic uplift derived from coral growth in the Batu Islands area [*Sieh et al.*, 1999] seem to require a LFZ extending potentially below the forearc Moho. In this study, we take advantage of an augmented and revised coral data set [*Natawidjaja et al.*, 2004], and from new available GPS measurements [*Bock et al.*, 2003] to analyze in more details this particular example, focusing on the geometry of the plate interface and position of the downdip end of the LFZ with respect to the forearc Moho.

[4] Hereafter we first summarize the geodynamical and geological setting of the study area. We next discuss the position of the forearc Moho at the plate interface based on a two-dimensional (2-D) gravimetric modeling of our study area, and present our elastic modeling approach to finally compare the inferred kinematics with the probable forearc structure and some thermal models of the subduction zone. We find that the LFZ extends below the 30 km deep forearc Moho, to a depth of ~46 km where the temperature is estimated to 260 ± 100°C. Finally, we discuss the significance of this finding.

2. Geodynamical Context

[5] The Batu Islands (Figure 2) lie along the Sumatra subduction zone where the oblique convergence between the Indo-Australian plate and the Sunda block partitions into a dip-slip component and a right-lateral strike-slip component, accommodated respectively on the subduction interface and on the Sumatran Fault [*Fitch*, 1972]. In central Sumatra, two major thrust events occurred in 1833 ($M \sim 9$) and 1861 ($M \sim 8.5$), which may have ruptured the subduction interface to depths of the order of 40–50 km [*Newcomb and McCann*, 1987] (Figure 2). More recently, the 1935 (M_w 7.7) and 1984 (M_w 7.2) thrust events ruptured smaller patches of the subduction interface at the boundary between the 1833 and 1861 earthquakes [*Rivera et al.*, 2002] (Figure 2); the ruptured surface involved in both recent events extended to depths greater than the 27 km deep

hypocenter, probably to depths of ~35–40 km. The Batu Islands are located in the area where the Investigator Fracture Zone (IFZ) subducts beneath Sumatra (Figure 2); the IFZ separates oceanic crust aged ~53 Myr old to the west from oceanic crust aged ~65 Myr old to the east [*Liu et al.*, 1983].

[6] Previously interpreted as the emerged portion of the active accretionary prism [*Moore and Karig*, 1980], the islands that lie between the coast and the trench are now considered as part of the forearc [*Samuel*, 1994; *Samuel et al.*, 1995]. The location of these islands, (~90–160 km from the trench) is ideal to study subduction zone processes from surface deformation. Interseismic straining is documented by GPS campaign measurements from 1991 to 2001 [*Bock et al.*, 2003], and by the pattern of uplift derived from coral growth over the period 1962–2000 around the Batu Islands [*Natawidjaja et al.*, 2004] (Figures 2 and 3). The GPS data set does not show any significant lateral variations that may correlate with any structural complexity suggested in previous studies [*Prawirodirdjo et al.*, 1997]. To the first order, a 2-D analysis of interseismic strain seems appropriate in this region. The coral data put relatively tight constraints on the downdip end of the LFZ, since the maximum uplift rate lies more or less above the transition zone to aseismic slip. This location indicates that the LFZ extends to ~130–140 km from the trench, and is roughly consistent with the fact that centroid moment tensor (CMT) catalog shows dominantly thrust events updip of this point, to depths of the order of 50 km, and downdip tension at greater depths (Figure 3). The plate interface is only poorly constrained from relocated seismicity [*Engdhal et al.*, 1998], but its seems plausible that the LFZ extends deeper than the forearc Moho.

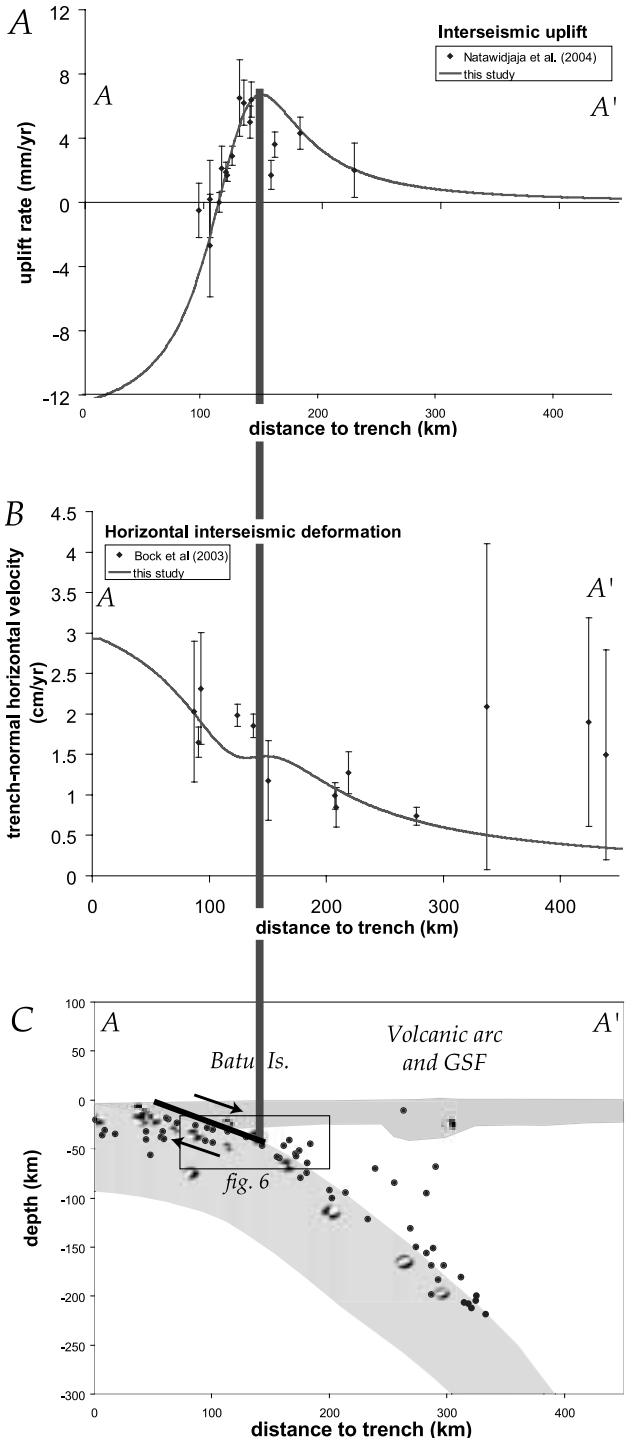

Figure 3. Seismicity and interseismic deformation along section A-A′ (see location in Figure 2). Theoretical interseismic velocities were calculated using a back slip model [*Savage*, 1983] with the set of best fitting parameters, that is, a downdip end of the LFZ 132 km from the trench and 46 km deep. Uncertainties are given at the 95% confidence level for observed data. The zone of maximum uplift is indicated by the thick vertical line over the three sketches. (a) Uplift rates relative to the stable margin of Sumatra derived from revised coral growth [*Natawidjaja et al.*, 2004] at the sites shown in Figure 2. Both calculated and observed vertical velocities include an eustatic correction of 2.4 mm yr^{-1} [*Peltier and Tushingham*, 1989]. (b) Horizontal velocities relative to the Sunda Shelf derived from the GPS measurements [*Bock et al.*, 2003]. (c) Seismicity [*Engdhal et al.*, 1998] and Harvard's CMT focal mechanisms along our trench-normal profile, with a forearc crustal structure as inferred from seismic refraction [*Kieckhefer et al.*, 1980] and gravimetric modeling (this study). The back slip dislocation of our preferred model is reported: the downdip extension of our dislocation is consistent with the expected deep limit of the LFZ from coral data. This geometry is consistent with earthquakes focal mechanisms (CMT catalogue) that indicate thrust events updip of the LFZ, and downdip tension at greater depths. Box shows location of the zone represented on Figure 6. GSF, Great Sumatran Fault.

3. Forearc Crustal Structure

[7] Here we analyze the position of the forearc Moho beneath the islands, which is a critical datum to our study. Seismic refraction investigations in the Nias Island area have documented the forearc crustal structure [*Kieckhefer et al.*, 1980]. The main velocity contrasts are reported on Figure 4. The sediment cover, with velocities of ~2 km s^{-1}, only appears seaward from the trench before sediments get integrated into the accretionary wedge (2.3–4.9 km s^{-1})

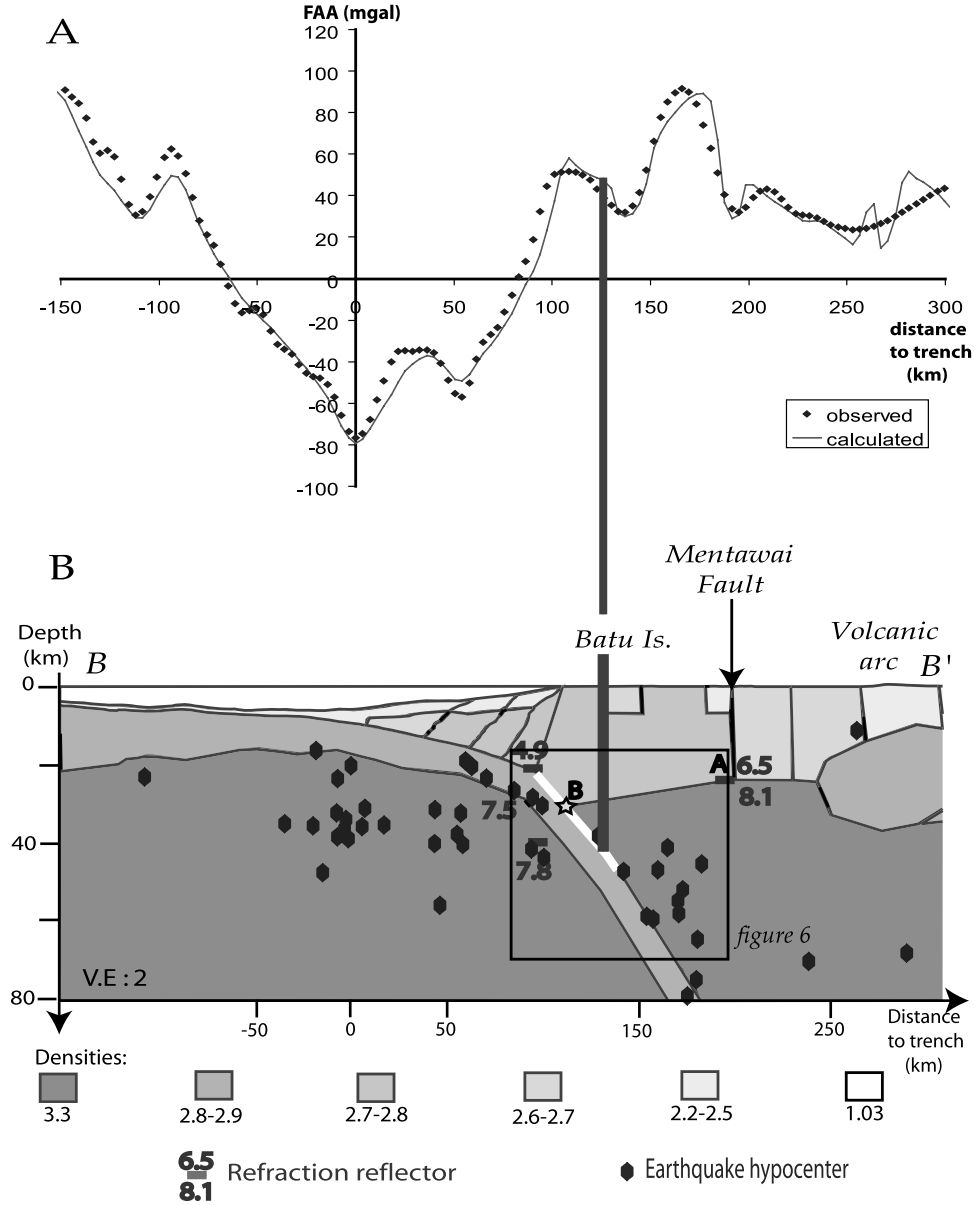

Figure 4. Gravimetric modeling, with model geometry and gravimetric anomalies along profile B-B′ (Figure 2 insert). The zone of maximum interseismic uplift is indicated by the thick vertical line. (a) Free-air anomalies (FAA) calculated for our preferred model, compared to anomalies observed from satellite altimetry [*Sandwell and Smith*, 1997]. According to our preferred model the forearc Moho intersects the subduction interface at a distance of 110 km from the trench and a depth of 30 km. (b) Gravimetric model geometry, based on bathymetry measured from satellite altimetry [*Sandwell and Smith*, 1997], seismic refraction data [*Kieckhefer et al.*, 1980], and seismicity [*Engdhal et al.*, 1998]. Major refraction interfaces are reported with the corresponding velocity, along with seismicity. Point A locates the 23 km deep forearc Moho documented by *Kieckhefer et al.* [1980]. The location of the Moho at the plate interface is indicated by point B; its tested position was varied along the white line, corresponding to depths between 21 and 55 km. Box shows location of the zone represented in Figure 6. A vertical exaggeration of 2 was applied for easier reading.

offshore Nias Island, whereas the oceanic crust (layer 2, ~5.2 km s^{-1}, and layer 3, 6.2–7.5 km s^{-1}) may be followed almost continuously from the trench to depths of ~40 km at a distance of ~100 km from the trench. The 4.9–7.5 km s^{-1} velocity contrast seaward from the island is consistent with the top of the downgoing slab that can be inferred from seismicity data [*Engdhal et al.*, 1998] (Figure 4). The 7.5–7.8 velocity contrast at 42.7 km depth reported by *Kieckhefer et al.* [1980] seaward from Nias most probably marks the Moho of the downgoing oceanic crust. On the forearc side, the Moho is constrained ~180 km from the trench, below the Nias basin, at a depth of 23 km

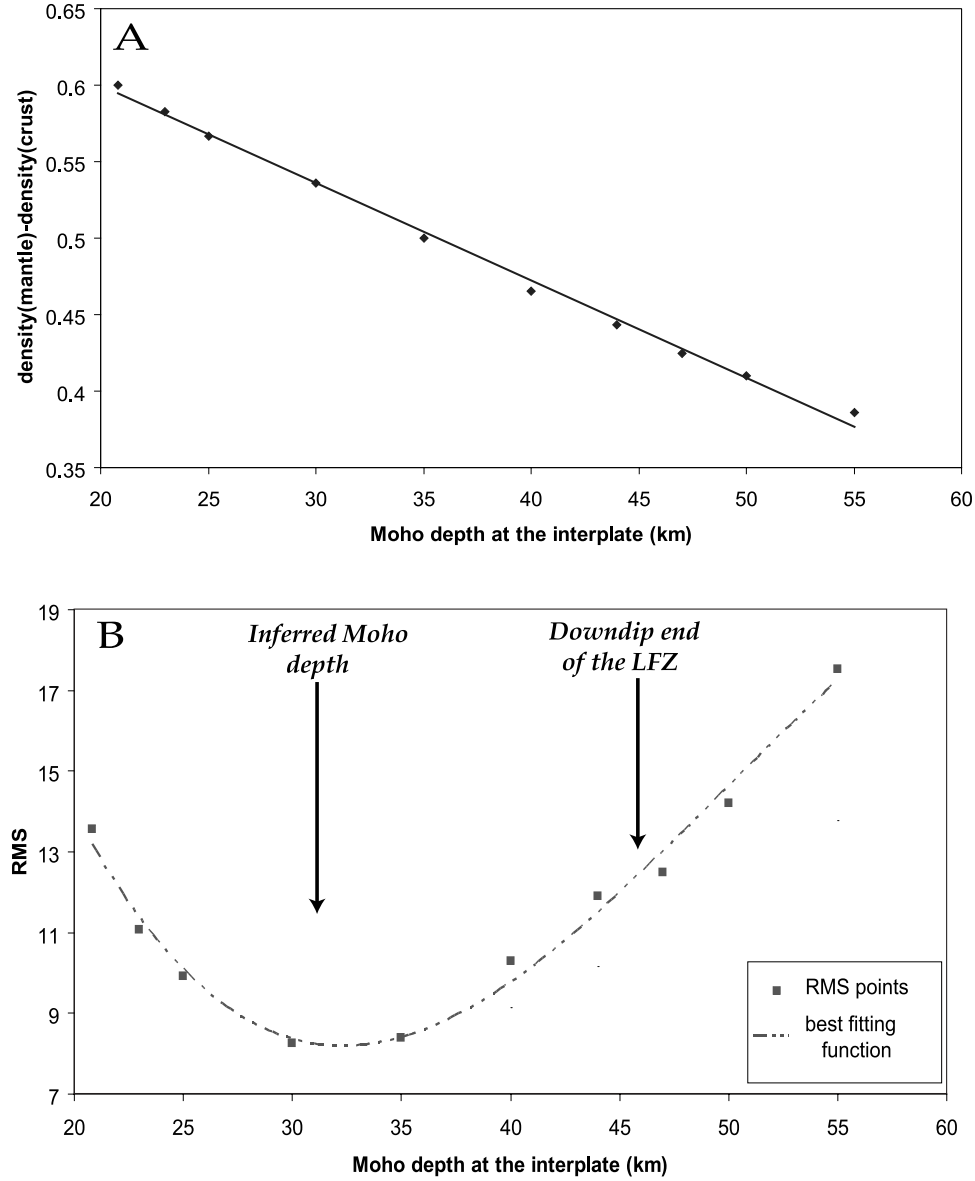

Figure 5. Gravimetric model results for the depth of the Moho at the plate interface. (a) Density contrasts at the Moho beneath the Batu Islands needed to fit the observed anomalies for varying depths of intersection of the forearc Moho with plate interface (point B in Figure 4). There is a clear trade-off between these two parameters. (b) Root minimum square (RMS) between observed and calculated anomalies for each one of the gravimetric models tested. RMS was computed in the area of interest between the trench and the Sumatran coastline. The RMS is minimum for a Moho depth of $\sim$30–32 km.

from a 6.5–8.1 km s^{-1} velocity contrast (Figure 4). The forearc crustal thickness is a critical datum to the gravimetric modeling that we performed hereafter in order to better constrain the Moho depth at the intersection with the plate interface. The 23 km deep velocity contrast might be questionable since an unmodeled early arrival in Figure A11 of *Kieckhefer et al.* [1980] would me more consistent with a $\sim$6.5 km s^{-1} thicker forearc crust; however, we believe that this arrival is not linked to any structural complexity since it does not appear in Figure A10 of *Kieckhefer et al.* [1980], which corresponds to the same line but shot in the opposite direction. Beneath the outer arc islands, the position of the Moho is not constrained from the refraction data, but gravimetric data can determine its geometry. *Kieckhefer et al.* [1981] proposed several models based on these seismic refraction data and on measured free-air anomalies. Two of these models assume that the 23 km deep Moho observed in the Nias basin [*Kieckhefer et al.*, 1980] belongs to the downgoing slab [*Kieckhefer et al.*, 1981, Figures 7 and 9]. This interpretation is difficult to reconcile with the local seismicity [*Engdhal et al.*, 1998] and can therefore be discarded. The alternative forearc model is more consistent with seismicity, and suggests a Moho that shallows from 23 km in the forearc basin to

~20 km near the intersection with the subduction interface. To get some idea of the uncertainty on this estimate, we have reanalyzed the gravimetric modeling.

[8] We considered a 2-D section perpendicular to the trench through the Batu Islands, just south of the Nias Island where the above studies have been performed. We used free-air anomalies and bathymetry derived from satellite altimetry [*Sandwell and Smith*, 1997] (http://topex.ucsd.edu) and modeled them with Hypermag [*Saltus and Blakely*, 1995] (ftp://ftpmusette.cr.usgs.gov/pub/). The 2-D hypothesis is justified from the dominantly northwest-southeast trench-parallel trend of gravity anomalies. We believe that lateral variations exist but are of minor importance for our purpose.

[9] We started from a model tied to the seismic refraction measurements around Nias [*Kieckhefer et al.*, 1980] (Figure 4). A uniform density of 2.89 was assumed for the whole downgoing oceanic crust [*Carlson and Raskin*, 1984], while a density of 3.3 was assigned to the mantle. For the accretionary prism we used densities in the range of values inferred from the refraction velocities using the Nafe-Drake curve [*Ludwig et al.*, 1970]; as noticed by *Kieckhefer et al.* [1981], some slightly larger densities were needed. The crustal structure on mainland Sumatra is not critical for our analysis and was adjusted to the first order. We considered a relatively light upper crust (2.38–2.48), with a denser (2.87–2.88) ~35 km deep magmatic basement [*Masturyono et al.*, 2001] beneath the volcanic arc. Densities of ~2.65 were assumed for the landward part of the forearc basin, between the Mentawai Fault and the coastline. The Moho was set there to a depth of 23 km based on seismic refraction data [*Kieckhefer et al.*, 1980] (point A in Figure 4). We varied the depth of the Moho at the intersection with the plate interface (point B in Figure 4) between 21 and 55 km. The density of the crust between the accretionary prism and the Mentawai fault was locally adjusted so as to best fit the gravity data. A clear trade-off appears between the density contrast at the Moho and the depth of point B (Figure 5a), and inferred crustal densities are still realistic for the whole range of Moho depths tested. However, the fit to the gravity data varies significantly. The best fit is obtained for a Moho depth of ~30 km located 110 km from the trench and a crustal density of ~2.764 ($\Delta\rho = 0.536$) (Figure 5b). We are aware that modeling the gravity data will not yield a unique solution and that we have not explored all possibilities of trade-offs. However, when all the data are considered together, including the refraction data and the seismicity, it makes it very improbable that the forearc Moho would intersect the subduction interface at a depth greater than ~35 km. A depth of ~30 km, at a horizontal distance of 110 km from the trench, seems most plausible.

4. Estimating the Location of the Downdip End of the Locked Fault Zone

4.1. Presentation of the Data on Interseismic Deformation

4.1.1. GPS Horizontal Velocities in the Forearc

[10] This study takes advantage of a recent reanalysis of all GPS data available around Indonesia in a consistent reference frame, the ITRF2000 [*Bock et al.*, 2003] (Figure 2). These data document the convergence between Sunda and Australia, as well as current strain along the subduction zone. According to this analysis, in the area of the Batu Islands, Australia and Sunda converge by 55.3 mm yr^{-1} with an azimuth of N12.3°, implying a trench normal velocity of 40.4 mm yr^{-1}. Interseismic deformation in our study area is documented from 13 stations (Figures 2 and 3). We considered these data together with their 95% uncertainties.

4.1.2. Uplift Data From Coral Growth

[11] Coral morphology may allow for an excellent time series reconstruction for tracking relative sea level history, providing a powerful tool to measure tectonic vertical deformation [*Taylor et al.*, 1987; *Zachariasen et al.*, 1999, 2000]. We based our analysis on *Natawidjaja et al.*'s [2004] data who augmented and revised the data set initially presented by *Sieh et al.* [1999], and paid particular attention to the estimation of uncertainties related to natural oceanographic fluctuations, and variable response of corals to relative sea level changes. We considered the data covering the 1962–2000 period. This data set does not show evidence either for any postseismic deformation following a silent event in 1962, or for coseismic deformation associated with the nearby 1984 earthquake (M_w 7.2) [*Rivera et al.*, 2002]. It might therefore be considered representative of deformation in the interseismic period. These coral data primarily indicate vertical displacement relative to sea level and are therefore a record of both tectonic deformation and sea level change (Figure 3). Taken at face value, these data show a maximum uplift rate at ~130–140 km from the trench, apparently well beyond the intersection of the plate interface with the forearc Moho 110 km from the trench. Moreover, the sharp peak advocates for an abrupt transition from the LFZ to the aseismic portion of the thrust fault, rather than for a wide transition zone that should produce a broad uplift peak as observed along the Nankai Trough [*Aoki and Scholz*, 2003]. The coral data closest to the trench seem to indicate that a shallow portion of the thrust fault may creep [*Natawidjaja et al.*, 2004]. In the following, as we did not try to model creep at the toe of the accretionary prism and only focused on the downdip extension of the LFZ, we did not account for such an eventual updip limit of the LFZ. We have tested, however, that including or discarding this datum had no effect on the determination of the downdip end of the LFZ.

[12] GPS and coral data do not cover the same observation period. This may be a problem if the interseismic phase is nonstationary; temporal variations of vertical deformation rates suggested by long time series of coral growth [*Natawidjaja et al.*, 2004] advocate for this nonstationarity, above all during the years just before and after a major earthquake such as the 1935 event. However, vertical data over 1962–2000 show a linear and spatially stable trend, supporting the stationary hypothesis for this time interval in our study area. Consequently, both data sets should be consistent and may be analyzed jointly.

4.2. Elastic Dislocation Modeling

4.2.1. Modeling Approach

[13] To determine the kinematics of interseismic deformation consistent with the GPS and coral data on interseismic straining, we adopted a simple back slip model

Table 1. Range of Values Explored in the Grid Search for the Best Fitting Parameters Defining the Back Slip Model

Data Considered	Range of Values
Distance to trench, km	70–200
Depth, km	15–70
Trench-normal velocity, mm yr^{-1}	10–70 (if not fixed)
Dip angle, deg	5–40
Eustatic correction, mm yr^{-1}	0–5 (if not fixed)

[*Savage*, 1983] using a 2-D analytical approximation of surface deformation for dip-slip faults [*Singh and Rani*, 1993]. On the basis of mid-Holocene coral fossils and on models of Holocene hydro-isostatic adjustments to deglaciation, *Zachariasen et al.* [1999, 2000] suggest that there has been no net significant vertical displacement over the past thousand years. This implies that coseismic and interseismic displacements balance each other over several seismic cycles. These observations support the hypothesis, inherent in the use of the back slip model, that there is negligible long-term deformation and that all strain accumulated elastically during the interseismic period is released by major earthquakes. The assumption of a purely elastic medium may be questionable. By comparing results from elastic dislocation models and viscoelastic models, we realized that the viscoelastic models are better at reconciling simultaneously horizontal displacements and vertical uplift rates, while dislocation models with abrupt transitions to aseismic slip at depth tend to predict a too narrow pattern of uplift rates, with a maximum value slightly offset trenchward; this is in particular apparent in the paper by *Vergne et al.* [2001]. A detailed analysis of the physical origin of a possible bias induced by elastic dislocation models is beyond the scope of this study; however, purely elastic dislocation models proved to be good approximations for interseismic and coseismic deformation since they provide similar results to viscoelastic finite element models [*Hyndman et al.*, 1995; *Vergne et al.*, 2001; *Wang et al.*, 1994]. For simplicity and because of the relatively narrow peak of uplift rates, we assumed an abrupt transition from the fully locked to the continuously sliding portion of the fault, rather than a zone of transition, along which slip rate would gradually taper to zero, and that could be taken to be linear [*Dragert et al.*, 1994; *Hyndman and Wang*, 1995; *Hyndman et al.*, 1995; *Oleskevich et al.*, 1999], exponential [*Wang et al.*, 2003] or random [*Darby and Beavan*, 2001]. Moreover, it should be noticed that these different transition models predict similar deformation patterns: the same deformation pattern might be obtained from a model with an abrupt termination of the LFZ than with a transition zone by extending the LFZ a bit deeper [*Hyndman and Wang*, 1995; *Hyndman et al.*, 1995].

4.2.2. Modeling Results

[14] We investigated systematically the space of parameters and computed the misfit with the observations from a χ^2 criterion, in which both GPS and coral data are weighted according to their 1σ standard deviation corrected so that the minimum χ^2 (hereinafter χ^2_{min}) for each data set inverted separately approximates the number of data (Tables 1, 2 and 3); the correction factor to the data uncertainties calculated from these separate inversions was then applied to the joined inversion of both interseismic

Table 2. Model Parameters Obtained From the Inversion of Either the Coral or the GPS Data or of Both Data Sets When All Five Parameters of the Model Are Inverted Jointly[a]

Data Considered	Number of Data	Correcting Factor for 1σ Data Uncertainties	χ^2_{min}	Distance to Trench, km	Depth, km	Trench-Normal Velocity, mm yr^{-1}	Dip Angle, deg	Eustatic Correction, mm yr^{-1}
Coral data	16	1.694	16.014	130 ± 10/5	15 ± 18/?	16 ± 10/?	17 ± 12/10	0 ± 2.5/?
GPS data	13	1.5377	13.014	94 ± 30/-?	39 ± 32/10	68 ± ?/42	31 ± ?/?	—
Coral and GPS data	29	1.694 (corals) 1.5377 (GPS)	74.605	125 ± 15	50 ± 15/5	44 ± 16/8	19 ± 12/8	5 ± ?/1

[a]Error bars indicate 95% confidence levels. When the range of values corresponding to this confidence level exceeds the explored space of parameters, a question mark is indicated in the uncertainties.

Table 3. Model Parameters Obtained From the Inversion of Either the Coral or the GPS Data or of Both Data Sets[a]

Data Considered	Number of Data	Correcting Factor for 1σ Data Uncertainties	χ^2_{min}	Distance to Trench, km	Depth, km	Trench-Normal Velocity, mm yr^{-1}	Dip Angle, deg	Eustatic Correction, mm yr^{-1}
Coral data	16	2.529	16.743	105 ± 17/16	61 ± ?/24	40.4 (fixed)	38 ± 2/8	1.2 (fixed)
GPS data	13	1.694	13.028	103 ± 23/?	52 ± ?/14	40.4 (fixed)	5 ± 9/?	—
Coral and GPS data	29	2.529 (corals) 1.694 (GPS)	73.493	132 ± 7	46 ± 16/11	40.4 (fixed)	20 ± 4/3	2.4 (fixed)
Coral and GPS data	29	2.529 (corals) 1.694 (GPS)	95.936	133 ± 9/6	47 ± 20/12	40.4 (fixed)	22 ± 3	1.2 (fixed)
Preferred values				132 ± 10/7	46 ± 11/9	40.4 (fixed)	20 ± 5/3	2.4 and 1.2 (fixed)

[a]In these inversions, the trench-normal velocity and eustatic correction are fixed to values estimated from other regional or global constraints [*Bock et al.*, 2003; *Peltier and Tushingham*, 1989]. Error bars indicate 95% confidence levels. When the range of values corresponding to this confidence level exceeds the explored space of parameters; a question mark indicates uncertainties. The range of preferred values for the location of the downdip end of the LFZ was estimated by assuming both extreme values for the eustatic correction.

straining data. This weighting, along with the similar size of both data sets, favors an equal contribution of GPS and coral data to the final solution. It should be recalled that the geometry of the back slip dislocation does not need to match the real geometry of the locked fault zone, but only needs to be tangent to the slab at the transition from slip strengthening to slip weakening [*Dragert et al.*, 1994; *Vergne et al.*, 2001]. Because coral growth depends both on local uplift and sea level variations, the model parameters are: the dip angle of the back slip dislocation, the position of the downdip end of the LFZ (distance to the trench and depth), the trench-normal convergence rate, and the eustatic correction on the coral data. From the pattern of interseismic uplift, the downdip end of the dislocation is expected to be at ~110–130 km from the trench; when compared with the slab geometry inferred from seismicity, this horizontal position corresponds to a depth of ~40 km. Seismicity also provides some constraints on the dip angle; because the downdip end of the LFZ is expected to be deeper than the 1984 earthquake hypocenter [*Rivera et al.*, 2002], the dip angle should be at least equal to the 12° focal plane solution, and probably steeper. Different plate models for the Sunda block yield a wide range of convergence velocities in our study area, from ~25–30 mm yr^{-1} up to ~70 mm yr^{-1} [e.g., *Simoes*, 2002]; the most recent GPS data in the region favor a 40.4 mm yr^{-1} convergence rate normal to the trench [*Bock et al.*, 2003]. Also, the plate interface might not be fully locked, so that the inversion of the interseismic straining data could reflect a trench-normal velocity lower than the actual plate convergence. As for the eustatic correction, *Peltier and Tushingham* [1989] suggest a sea level rise between 1.2 and 2.4 mm yr^{-1}. To check the validity of our approach and of such a simple model, we have decided to first let the different model parameters vary within a wide range of possible values (Table 1). In addition to determining the best fitting set of parameters, from the value of χ^2_{min}, we determine the 95% confidence level on each parameter (Tables 2 and 3).

[15] We first explored the possibility to constrain all five parameters of the model from the local interseismic straining data. To assess the different constraints provided by the two different data sets, the GPS and coral data were initially inverted separately (Table 2). The model parameters which best fit the coral data (Table 2) imply a convergence rate of only 15 mm yr^{-1}, clearly too low in view of the 40.4 mm yr^{-1} convergence determined by *Bock et al.* [2003] from a much broader network than the one used in our inversion, and a depth for the downdip end of the LFZ of 15 km, too shallow in view of the various constraints on the location of the plate interface. Also, this model would imply a 0 mm yr^{-1} eustatic correction, which is unrealistic. This results from the coral data on the landward side of the uplift peak, between 160 and 230 km from the trench, which show some inconsistency (Figure 3). A more complex model is needed to fit better the data, but it is beyond the scope of this study. On the other hand, the GPS data, when inverted separately, allow trade-offs between the depth and the distance to the trench of the downdip end of the LFZ yielding a large range of possible velocities and dip angles (Table 2), so that the characteristics of the LFZ may not be well resolved by only such data. Despite the fact that the χ^2_{min} values for both separate GPS

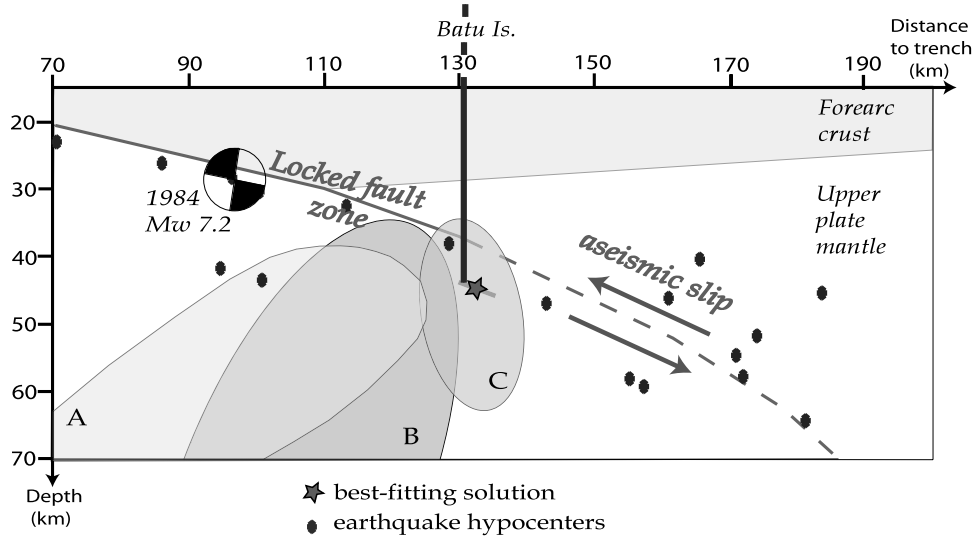

Figure 6. Determination of the position of the downdip end of the LFZ: best fitting solution with 95% confidence level domains determined from the χ^2 criterion inferred from GPS data (domain A), coral data (domain B), and both data sets (domain C) when the convergence rate and the eustatic correction are set to 40.4 and 1.2–2.4 mm yr^{-1}, respectively (Table 3). The horizontal position and the depth of the downdip end of the LFZ varied within the domains represented by the figure. GPS and coral data define overlapping 95% confidence intervals that are larger than the computed space of parameters: indeed, their uncertainties were almost doubled for the inversion. The joined inversion yields a well-defined domain of possible locations of the downdip end of the LFZ, especially for the horizontal position. This latter is consistent with the zone of maximum uplift (thick vertical line). Seismicity from *Engdhal et al.* [1998] and the position of the forearc Moho from gravimetric modeling (Figure 4) are reported. The 1984 earthquake focal mechanism [*Rivera et al.*, 2002] was also projected on section A-A′.

and coral data are comparable, their 95% confidence intervals do not overlap well. We believe the apparent inconsistency between the two data sets could most probably be due to the modeling approach. When both data sets are inverted jointly, with corrected uncertainties as calculated in their respective separate inversions, the best fitting model yields reasonable values for the different parameters except for the eustatic correction which seems too small compared to global estimates [*Peltier and Tushingham*, 1989] (Table 2). Because of the difficulty in reconciling well the two data sets despite normalized uncertainties, the χ^2_{min} value is relatively large in the case of the joined inversion. These different tests underline the limitations of the different data when interpreted within a simple model, as well as the insufficient resolution when two many parameters are inverted.

[16] In our final models we take into account additional constraints to limit the freedom on the model parameters. Namely, we impose a convergence rate of 40.4 mm yr^{-1} [*Bock et al.*, 2003] and assume an eustatic correction either in the upper range, 2.4 mm yr^{-1}, or lower range, 1.2 mm yr^{-1}, of possible values [*Peltier and Tushingham*, 1989]. We are then left with only three free parameters: the location (X, Z) of the downdip end of the LFZ and the dip angle of the dislocation. By imposing such convergence rate, we assume that the LFZ is fully locked during the interseismic period, so that shortening between the two plates may not be accommodated by any aseismic slip; however, consistency of the results with available constraints confirms this hypothesis. As previously, GPS and coral data were first inverted separately (Table 3). The 95% confidence intervals for the depth of the downdip extension of the LFZ and for the dislocation dip exceed the space of investigated values in both inversions (Figure 6). Despite these large uncertainties, the two data sets considered separately define overlapping domains of possible values for the model parameters (at the 95% confidence level) (Figure 6). It should be noticed that the GPS data can be fitted from a variety of models due to the trade-off between the horizontal position and the depth of the creeping dislocation (Figure 6). The coral data do not show such a trade-off, and despite the large uncertainties in the depth, they put tighter constraints on the distance to the trench of the downdip end of the LFZ. However, within such a simple modeling approach, it seems that coral data require additional constraints to solve for the characteristics of the LFZ and to provide consistent results. Finally, on the basis of the joined inversion of both coral and GPS data, we estimate that the downdip end of the LFZ must be located at a horizontal distance from the trench of 132 ± 10/7 km (Figure 6). This well-constrained position coincides well with the zone of maximum interseismic uplift, which is, as stated previously, a good model-independent indicator of the position of the downdip limit of the LFZ. The fault dip angle (20 ± 5/3°) is consistent with the Benioff zone, and somehow steeper than the shallower 12° thrust plane of the 1984 earthquake [*Rivera et al.*, 2002], as expected. The

Table 4. Parameters for the 2-D Thermal Models of Figures 7 and 8[a]

Model	Shear Heating	Radiogenic Heat Production, $\mu W\ m^{-3}$	Volcanic Arc (Landward Boundary Condition)	Predicted Heat Flow at 25 km From the Trench, Mw m^{-2}	Predicted Heat Flow off Nias Island, mW m^{-2}
A	yes	2.5	yes	37.6	50.5
B	yes	2.5	no	37.6	50.5
C	yes	0.4	yes	32.4	22.2
D	no	0.0	yes	27.6	10.1
E	no	0.4	no	27.9	13.8
F	no	0.0	no	27.6	10.1

[a]A convergence velocity of 40.4 mm yr^{-1} [*Bock et al.*, 2003] was considered for all models. Some predicted heat flows are reported for each model; these values can be compared to the 44.4 mW m^{-2} measured at 25 km from the trench [*Vacquier and Taylor*, 1966] and to the 28 mW m^{-2} off Nias [*Pollack et al.*, 1993]. Radiogenic heat production for models C and E is chosen after *Hyndman and Wang* [1993] for the accreted terranes of the Cascades. Model C, obtained with realistic radiogenic heat production, predicts heat flows that are the most compatible with those measured (Figure 7): it is therefore our preferred model.

depth of 46 ± 11/9 km seems reasonable, yet a bit deep, compared to other constraints on the plate interface. This is the consequence of assuming an abrupt transition from the LFZ to the continuously sliding portion of the plate interface. A value, around 40–42 km, in the upper range of the 95% confidence level, would be more plausible. Figures 3 and 6 illustrate these results and how they compare with the thrust geometry at the transition to aseismic slip at depth. Surprisingly, the preferred location of the downdip end of the LFZ lies outside the position allowed by the 95% confidence intervals for the coral-only and the GPS-only models (Figure 6). This results from the very different range of dip angles obtained from the respective inversions of the coral or the GPS data (Table 3). The combined inversion leads to a dip angle significantly greater than the value deduced from the GPS data, and significantly lower than the value obtained from the coral data. In both cases the downdip end of the LFZ is forced to a more landward position (Table 3) and finally lies outside the confidence limits deduced from the separate inversions. This suggests that although the coral data put tighter constraints on the position of the landward extent of the LFZ, the inversion of interseismic data using a simple back slip model only yields realistic results when both vertical and horizontal straining data are used together. Predicted and observed horizontal and vertical interseismic velocities are also reported on Figure 3. Our preferred model fits well the GPS and coral data (Figure 3a) except for the two lower vertical velocities at ~160 km from the trench; as stated above, reconciling all vertical data on the landward side of the uplift peak is impossible with a simple back slip model, since there might be some along-section complexities. We have tested that including or removing these two data does not lead to significantly different values of the model parameters. We therefore chose to still consider them in our final results.

[17] The joined inversions suggest thus that the LFZ extends to a distance of 132 ± 10/7 km from the trench, which corresponds to a depth of 46 ± 11/9 km. The dip angle of the dislocation inferred from our study is of 20 ± 5/3°. Consequently, a back slip model with a slip rate close to the plate convergence velocity reconciles the vertical and horizontal data relatively well to the first order. We do not see any evidence for partial coupling along the plate interface that could have resulted from the fact that the subducting IFZ might carry hydrated minerals (supposed to favor aseismic slip) along the plate interface. In addition to that, this analysis confirms that, in the study area, the transition from the locked fault portion to the aseismic zone probably occurs downdip of the intersection of the plate interface with the forearc Moho (Figure 6).

5. Thermal Structure

[18] *McCaffrey*'s [1997] study suggests that Sumatra is a cold subduction zone; however it does not specifically assess the temperature at the downdip end of the LFZ which is of most importance to discuss the probable physical factors controlling the transition to aseismic slip at depth. Therefore the thermal structure of the Sumatra subduction zone was reanalyzed more precisely in our study.

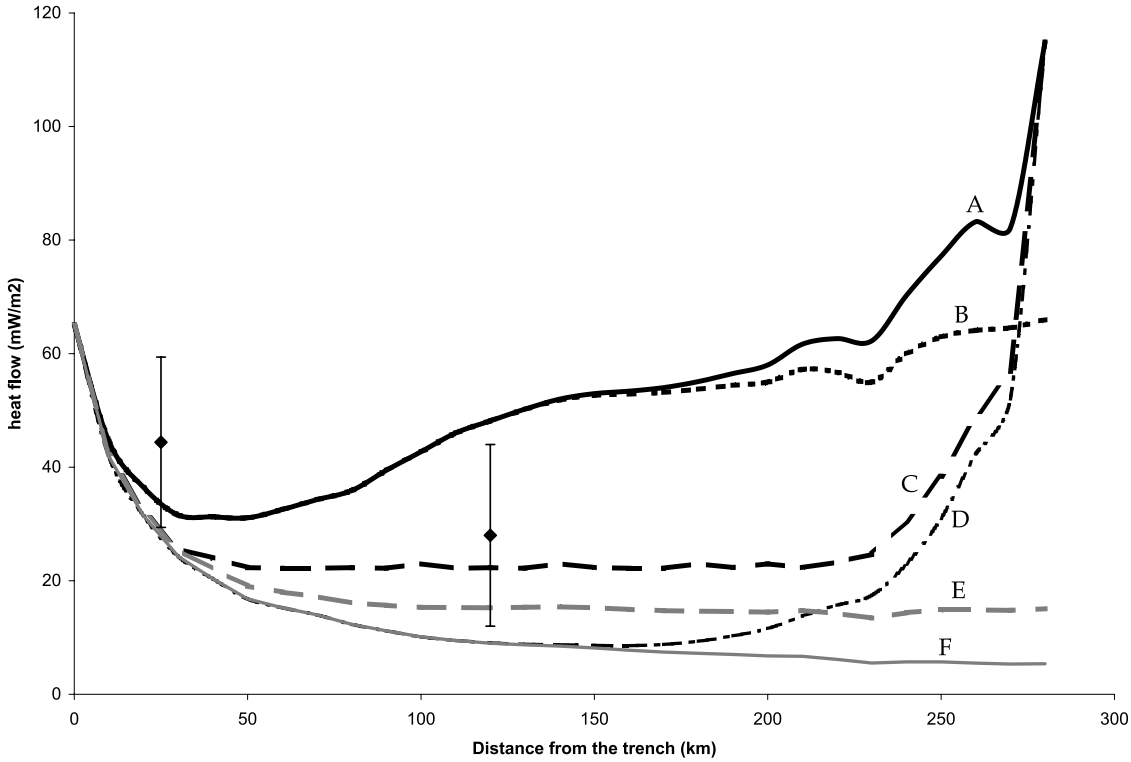

Figure 7. Heat flow computed from the thermal models described in Table 4. The two available measurements in our study area [*Pollack et al.*, 1993; *Vacquier and Taylor*, 1966] (Figure 2) were also reported. No uncertainty has been ascribed to these values. We have arbitrarily ascribed to these data uncertainties twice as large as those assigned to more recent similar measurements performed along the Kermadec forearc [*Von Herzen et al.*, 2001]. Model C, which assumes some shear heating at the plate interface, predicts heat flows that are the most compatible with the available data: it is therefore our preferred model. Also, it appears that the landward boundary condition does not influence significantly the thermal structure of the subduction zone in the zone closest to the trench where interseismic straining is most significantly being accumulated.

[19] The 2-D steady state thermal structure is modeled using the finite element method described by *Henry et al.* [1997] based on work by *Zienkiewicz and Taylor* [1989]. Two heat flow measurements are available in the study area, one at 25 km from the trench (44.4 mW m^{-2}) and the other off Nias Island (28 mW m^{-2}) [*Pollack et al.*, 1993; *Vacquier and Taylor*, 1966] (Figure 2). Although no uncertainty is ascribed to these values, we assume that they might be representative of the thermal structure around the down-dip limit of the locked fault zone; for reference, recent published measurements in other similar geodynamical contexts are ascribed uncertainties typically of the order of 5–6 mW m^{-2} for the same range of values [*Von Herzen et al.*, 2001]. The other values, all on the island of Sumatra, may be affected by the volcanic arc and by the Sumatran Fault. We computed a wide range of possible thermal structures, and, for qualitative comparison, the theoretical heat flow expected at these two structural distances from the trench (Table 4 and Figure 7). Figure 8 illustrates for each model the interplate temperature; the Moho location and the 350–450°C isotherms were also indicated for comparison.

[20] The model accounts for radiogenic heat production. Frictional shear heating is either neglected (models D, E, and F) or computed assuming an effective coefficient of friction of 0.1 within the brittle domain (models A, B, and C). Shear stress varies with depth according to the temperature-dependent rheological properties of the interplate constituents. Heat produced by metamorphic reactions or carried by fluids is neglected; besides, the thermal effect of accreted and downgoing sediments as well as erosion are not considered in this modeling. The slab geometry, based on the seismicity [*Engdhal et al.*, 1998], is kept constant during all experiments. The thermal structure of the subducting lithosphere corresponds to a 53 Myr age [*Liu et al.*, 1983] and thus to a 95 km thickness. The forearc crustal structure is modeled after the best fitting gravity model of this study. The trench-normal velocity is fixed at 40.4 mm yr^{-1}. Temperature at the surface is 0°C and 1300°C at the base of the downgoing oceanic lithosphere. At the seaward boundary of the model, the vertical temperature gradient is calculated for a 53 Myr old oceanic lithosphere according to a simple 1-D cooling model [*Turcotte and Schubert*, 2002]; the surface heat flow predicted by this model is consistent with measured values seaward from the trench (~70 mW m^{-2}) [*Vacquier and Taylor*, 1966]. Following *Oleskevich et al.* [1999], we tested two possible boundary conditions at the landward side: models A and D have an imposed vertical

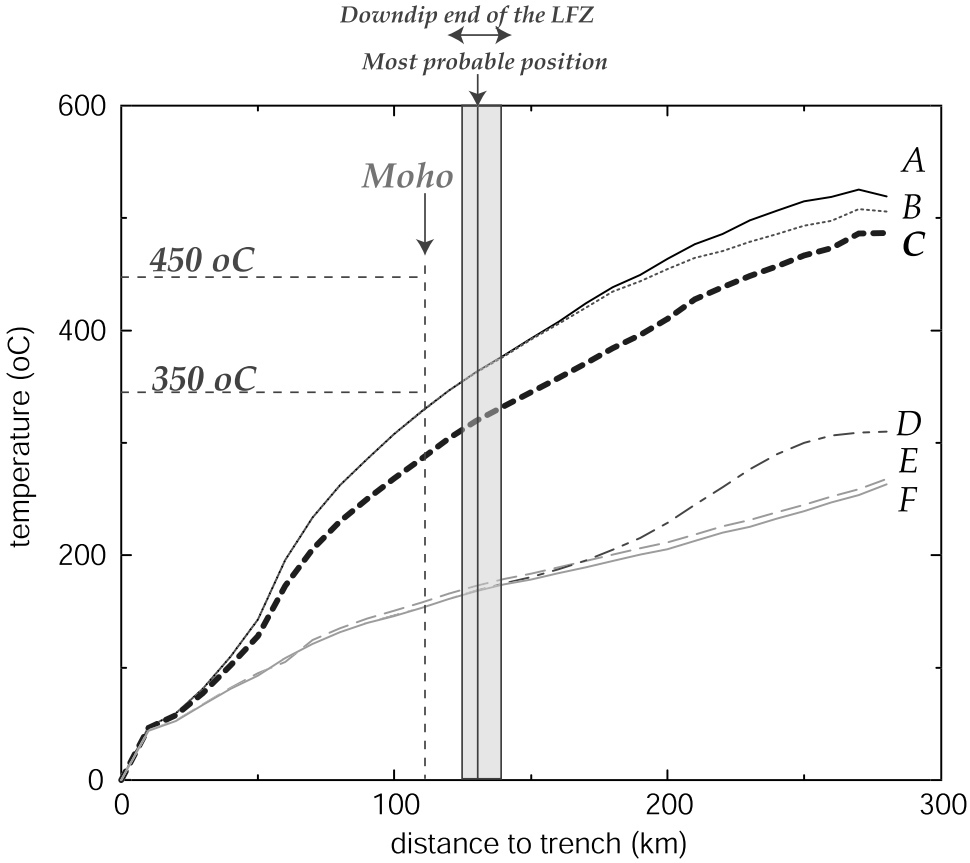

Figure 8. Temperatures along the subduction interface versus distance from the trench computed from the models described in Table 4. The position of the forearc Moho and the location of the downdip end of the seismogenic zone are indicated. The temperature above the Moho is well below the temperature needed for ductile flow (~450°C) or even stable sliding of quartzo-feldspathic rocks (~350°C) [*Blanpied et al.*, 1991, 1995]. Model C is our preferred model in view of the predicted heat flow (Figure 7). The transition to aseismic creep occurs around 310°C in the mantle, at a temperature well below the temperature needed for ductile flow of mantle rocks or mafic crust (~750–800°C).

temperature gradient to match the heat flow data on Sumatra Island, so as to account for the volcanic arc and the Sumatran Fault; models B, C, E and F assume zero horizontal heat flow across the landward boundary. Because this boundary is relatively far (280 km) from the trench, the assumed boundary condition has little effect on the temperature around the downdip end of the LFZ (Figure 8) and on the heat flow predicted in the area close to the trench (Figure 7). The thermal conductivity of the upper plate crust is taken to be 1.95 W m^{-1} K^{-1} [*Pollack et al.*, 1993]. Upper plate crustal densities are fixed at 2.764. The oceanic lithosphere is considered as nonradiogenic and is ascribed a density of 3.2, a thermal conductivity of 2.9 W m^{-1} K^{-1}, and a thermal capacity of 3.3 MJ m^{-1} K^{-1} [*Dumitru*, 1991]. We tested various extreme values for the radiogenic heat production in the forearc crust, since there are no data available.

[21] The hottest models (A and B of Table 4 and Figures 7 and 8) were obtained with a high radiogenic heat production of 2.5 μW m^{-3} for the whole forearc crust, and with shear heating. The coldest models (D and F of Table 4 and Figures 7 and 8) are obtained assuming a nonradiogenic upper plate and no shear heating. The combination of these different parameters resulted in four extreme thermal models of the Sumatran subduction zone. Models C and E of Table 4 are the most probable: they are both determined with realistic values for radiogenic heat production (comparable to the values proposed for example for the Cascadia subduction zone [*Hyndman and Wang*, 1993]), but shear heating is only introduced in model C. The really cold models might be discarded in view of the really small heat flows predicted (Table 4 and Figure 7). As observed in other island arc settings, such as the Kermadec [*Von Herzen et al.*, 2001] or the northeast Japan trench [*Peacock and Wang*, 1999], reasonable values of heat flow in the forearc can only be obtained with some amount of shear heating. Models A, B, and C might therefore seem more realistic although they include some shear heating probably in the upper range of what can be proposed. They correspond to a frictional shear stress of the order of 70 MPa, which is ~7 times larger than the value proposed along the Kermadec subduction zone for example. Model C, which in addition assumes a realistic low radiogenic heat production, predicts heat flows that are the most compatible altogether with the measured ones (Figure 7), although the misfit with the heat flow measurement at 25 km from the trench is not negligible; in any case,

uncertainties on the measurements are not given, and our models only aim at presenting a first order thermal structure of the Sumatra subduction zone given the several unknowns. Considering all these models, model C seems the most realistic. On the basis of all the results presented in Figure 8, we estimate that the range of possible temperatures near the downdip end of the locked fault portion (at ~46 km depth) is wide, probably between 160 and 360°C, with a more probable value around 310°C based on model C. Unfortunately, the available constraints on the thermal structure are too loose to get a more accurate estimate.

6. Discussion

[22] According to the kinematic models of interseismic straining discussed here, it is most probable that the LFZ extends deeper than the forearc Moho. This is consistent with the fact that none of the thermal models predicts temperatures higher than ~220°C within the crust. The crust is too thin and the subducting plate too cold to allow for significant ductile deformation or even for stable sliding of quartzo-feldspathic rocks [*Blanpied et al.*, 1991, 1995]. On the other hand, the fact that the fault remains locked well below the Moho challenges the view that serpentinized mantle would allow stable sliding of the thrust fault interface. It may indicate that the forearc mantle is not serpentinized which would be consistent with the high mantle *Pn* velocity of 8.1 km s^{-1} observed in the Nias basin [*Kieckhefer et al.*, 1980]. This might be possible given that the PT conditions at the forearc Moho may not be high enough to drive dehydration of the basaltic crust [*Peacock*, 2000], which in turn also depends on its unknown initial state of hydration. Another explanation might be that the mantle wedge be indeed serpentinized but that the PT conditions might not allow stable sliding. There is indeed some indication that serpentinites might become slip weakening (allowing for stick-slip behavior) at temperatures higher than ~200°C [*Moore et al.*, 1997], so the relatively hot temperature below the Moho might provide an alternative explanation. However, little is known about the frictional behavior of such hydrous minerals especially at high pressure.

[23] Some insight about the physical process at the origin of the deep transition to aseismic slip might be gained from comparing the Sumatra case with some other case examples. Along the Japan Trench, the LFZ seems to extend to a depth of ~50–55 km [*Mazzotti et al.*, 2000], below the 20–25 km deep Moho [*Hayakawa et al.*, 2002; *Miura et al.*, 2003, 2001; *Takahashi et al.*, 2000]. Thermal modeling [*Peacock and Wang*, 1999] suggests a temperature of ~200°C at this location, while *Pn* velocities of ~7.3–7.5 km s^{-1} suggest partial serpentinization at the toe of the forearc mantle wedge [*Hayakawa et al.*, 2002; *Miura et al.*, 2003]; below the island arc crust, however, the mantle shows little evidence of serpentinization with *Pn* velocities of 7.9–8.0 km s^{-1} [*Miura et al.*, 2003; *Takahashi et al.*, 2000]. Along the eastern Aleutians, interplate thrust events seem to have initiated at depths of 35–41 km [*Tichelaar and Ruff*, 1993], below the ~20 km deep Moho [*Holbrook et al.*, 1999; *Lizarralde et al.*, 2002], suggesting also that the LFZ may also extend into the mantle. At such depths the temperature is estimated to 200–220°C [*Peacock and Hyndman*, 1999]. In these two examples, the uncertainty on the temperature around the transition to aseismic sliding was not estimated, and we believe that the range of possible values might actually compare to those estimated for the Sumatra case. The onset of aseismic sliding along the plate interface in the mantle thus seems to occur at a depth of ~40–45 km and a temperature of 200–300°C. This would also be consistent with the fact that along the continental margins where the LFZ ends at the Moho, such as Alaska and some parts of Chile, since these conditions are already reached at the Moho depth [*Oleskevich et al.*, 1999].

[24] Either ductile flow or transition from stick slip to stable sliding might account for this transition. In the case of Sumatra, the corresponding temperature is most probably below 360°C. Such a temperature seems too low to allow ductile deformation of mantle rocks. To check for this we have modeled interseismic deformation using ADELI, a finite element code which allows for any kind of nonlinear rheology [*Hassani et al.*, 1997] that can depend on the local prescribed temperature [*Cattin and Avouac*, 2000]. We considered the hottest possible temperature field (model A) and rheological properties of dry or wet olivine [*Hirth and Kohlstedt*, 1996]. It turns out that even for a wet olivine rheology, thermally activated ductile creep is not effective enough to accommodate aseismic slip at depth along the plate interface. A transition to stable sliding, still in the brittle field, is therefore a more probable mechanism. This transition might be pressure and/or temperature controlled through a direct effect on the frictional property of the interface, or indirectly through the effect of pore pressure. The transition might for example relate to dehydration of the uppermost basaltic layer of the slab or to metamorphic reactions that modify interplate constituents and thus interplate properties. The released fluids could affect the rheological and frictional properties of the interface or play a major role in other possible physical-chemical processes. Indeed, *Peacock* [2000] suggests that the temperature needed to induce significant dewatering of the basaltic crust, through porosity collapse, is in the range of 300–500°C. The temperature near the downdip end of the seismogenic zone in the Sumatra study area might reach this range. Also, according to petrological modeling of the evolution of the subducting slab [*Hacker et al.*, 2003a, 2003b], these PT conditions also correspond to the transition to jadeite lawsonite blueschist facies, within which continuous dehydration may take place.

7. Conclusion

[25] Interseismic uplift recorded by coral growth and horizontal velocities measured from GPS are used to assess the geometry of the locked portion of the Sumatra subduction zone. The vertical and horizontal data are reasonably well reconciled with a simple model in which the plate interface is fully locked over a significant width. We find that the LFZ extends to a horizontal distance of 132 ± 10/7 km from the trench, which corresponds to a depth of 46 ± 11/9 km. Gravimetric modeling, seismicity data and seismic refraction data show that the plate interface intersects the forearc Moho at a depth of ~30 km. Thus, in the study area, the transition from the locked fault portion to the

aseismic zone occurs probably downdip of the forearc Moho, which challenges a current view that the LFZ does not extend into the mantle because serpentinization of the mantle wedge would favor stable aseismic sliding. Comparison with a simple thermal model suggests that the transition from the locked fault zone to the creeping zone of the plate interface occurs at a temperature of ~310°C at most, still too low for ductile flow. This transition thus probably reflects a change of the frictional properties of the plate interface. Stable aseismic sliding downdip of the LFZ could result from the effect of temperature and/or pressure on the frictional properties of the interface or, alternatively, the influence of fluids released by dehydration of the subducting plate. This study thus appeals to some reappraisal of the physical processes that allow aseismic slip along subduction zones at depth, and hence that control the process of stress buildup during the interseismic period. Some more insight might be gained from the study of cold subduction zones with a thin upper plate.

[26] **Acknowledgments.** We wish to thank K. Sieh and D. Natawidjaja, from the California Institute of Technology (Pasadena, California) for fruitful discussions on the coral data as well as for corrections on the manuscript. We also wish to thank N. Chamot-Rooke from the Ecole Normale Superieure (Paris, France) for his interest in the results of this study, and H. Hebert from Laboratoire de Detection et de Geophysique (CEA, France) for very useful discussions on the marine geophysics data. This manuscript was also substantially improved thanks to comments and suggestions by J. Freymueller, M. Reyners, and the anonymous Associate Editor.

References

Aoki, Y., and C. H. Scholz (2003), Interseismic deformation at the Nankai subduction zone and the Median Tectonic Line, southwest Japan, *J. Geophys. Res.*, *108*(B10), 2470, doi:10.1029/2003JB002441.

Bergman, I., and S. Solomon (1988), Transform fault earthquakes in the North Atlantic: Source mechanism and depth of faulting, *J. Geophys. Res.*, *93*, 9027–9057.

Blanpied, M. L., D. A. Lockner, and J. D. Byerlee (1991), Fault stability inferred from granite sliding experiments at hydrothermal conditions, *Geophys. Res. Lett.*, *18*, 609–612.

Blanpied, M. L., D. A. Lockner, and J. D. Byerlee (1995), Frictional slip of granite at hydrothermal conditions, *J. Geophys. Res.*, *100*, 13,045–13,064.

Bock, Y., L. Prawirodirdjo, J. F. Genrich, C. Stevens, R. McCaffrey, C. Subarya, S. S. O. Puntodewo, and E. Calais (2003), Crustal motion in Indonesia from GPS measurements, *J. Geophys. Res.*, *108*(B8), 2367, doi:10.1029/2001JB000324.

Carlson, R. L., and G. S. Raskin (1984), Density of the ocean crust, *Nature*, *311*, 555–558.

Cattin, R., and J.-P. Avouac (2000), Modeling mountain building and the seismic cycle in the Himalaya of Nepal, *J. Geophys. Res.*, *105*, 13,389–13,407.

Darby, D., and J. Beavan (2001), Evidence from GPS measurements for contemporary interplate coupling on the southern Hikurangi subduction thrust and for partitioning of strain in the upper plate, *J. Geophys. Res.*, *106*, 30,881–30,891.

Dragert, H., R. D. Hyndman, G. C. Rogers, and K. Wang (1994), Current deformation and the width of the seismogenic zone of the northern Cascadia subduction thrust, *J. Geophys. Res.*, *99*, 653–668.

Dumitru, T. A. (1991), Effects of subduction parameters on geothermal gradients in forearcs, with an application to Franciscan subduction in California, *J. Geophys. Res.*, *96*, 621–641.

Engdhal, E., R. van der Hilst, and R. Buland (1998), Global teleseismic earthquake relocation with improved travel times and procedures for depth determination, *Bull. Seismol. Soc. Am.*, *88*, 722–743.

Fitch, T. J. (1972), Plate convergence, transcurrent faults and internal deformation adjacent to southeast Asia and the western Pacific, *J. Geophys. Res.*, *77*, 4432–4460.

Hacker, B. R., G. A. Abers, and S. M. Peacock (2003a), Subduction factory: 1. Theoretical mineralogy, densities, seismic wave speeds, and H_2O contents, *J. Geophys. Res.*, *108*(B1), 2029, doi:10.1029/2001JB001127.

Hacker, B. R., S. M. Peacock, G. A. Abers, and S. D. Holloway (2003b), Subduction factory: 2. Are intermediate-depth earthquakes in subducting slabs linked to metamorphic dehydration reactions?, *J. Geophys. Res.*, *108*(B1), 2030, doi:10.1029/2001JB001129.

Hassani, R., D. Jongmans, and J. Chery (1997), Study of plate deformation and stress in subduction processes using two-dimensional numerical models, *J. Geophys. Res.*, *102*, 17,951–17,965.

Hayakawa, T., J. Kasahara, R. Hino, T. Sato, N. Shinohara, A. Kamimura, M. Nishino, T. Sato, and T. Kanazawa (2002), Heterogeneous structure across the source regions of the 1968 Tokachi-Oki and the 1994 Sanriku-Haruka-Oki earthquakes at the Japan Trench revealed by an ocean bottom seismic survey, *Phys. Earth Planet. Inter.*, *132*(1–3), 89–104.

Henry, P., X. Le Pichon, and B. Goffe (1997), Kinematic, thermal and petrological model of the Himalayas: Constraints related to metamorphism within the underthrust Indian crust and topographic elevation, *Tectonophysics*, *273*, 31–56.

Hirth, G., and D. L. Kohlstedt (1996), Water in the oceanic upper mantle: Implications for rheology, melt extraction and the evolution of the lithosphere, *Earth Planet. Sci. Lett.*, *144*, 93–108.

Holbrook, W. S., D. Lizarralde, S. McGeary, N. L. Bangs, and J. B. Diebold (1999), Structure and composition of the Aleutian island arc and implications for continental crustal growth, *Geology*, *27*(1), 31–34.

Hyndman, R. D., and K. Wang (1993), Thermal constraints on the zone of major thrust earthquake failure: The Cascadia subduction zone, *J. Geophys. Res.*, *98*, 2039–2060.

Hyndman, R. D., and K. Wang (1995), The rupture zone of Cascadia great earthquakes from current deformation and the thermal regime, *J. Geophys. Res.*, *100*, 22,133–22,154.

Hyndman, R. D., K. Wang, and M. Yamano (1995), Thermal constraints on the seismogenic portion of the southwestern Japan subduction thrust, *J. Geophys. Res.*, *100*, 15,373–15,392.

Hyndman, R. D., M. Yamano, and D. A. Oleskevich (1997), The seismogenic zone of subduction thrust faults, *Island Arc*, *85*, 863–889.

Kieckhefer, R. M., G. G. Sho, and J. R. Curray (1980), Seismic refraction studies of the Sunda trench and forearc basin, *J. Geophys. Res.*, *85*, 863–889.

Kieckhefer, R. M., G. F. Moore, F. J. Emmel, and W. Sugiarta (1981), Crustal structure of the Sunda forearc region west of central Sumatra from gravity data, *J. Geophys. Res.*, *86*, 7003–7012.

Liu, C. S., J. R. Curray, and J. M. McDonald (1983), New constraints on the tectonic evolution of the eastern Indian Ocean, *Earth Planet. Sci. Lett.*, *65*, 331–342.

Lizarralde, D., W. S. Holbrook, S. McGeary, N. L. Bangs, and J. B. Diebold (2002), Crustal construction of a volcanic arc, wide-angle seismic results from the western Alaska Peninsula, *J. Geophys. Res.*, *107*(B8), 2164, doi:10.1029/2001JB000230.

Ludwig, W. J., J. E. Nafe, and C. L. Drake (1970), Seismic refraction., in *The Sea*, vol. 4, edited by A. E. Maxwell, pp. 53–84, Wiley-Interscience, Hoboken, N. J.

Masturyono, , R. McCaffrey, D. Wark, S. Roecker, N. Fauzi, G. Ibrahim, and N. Sukhyar (2001), Distribution of magma beneath the Toba caldera complex, north Sumatra, Indonesia, constrained by three-dimensional *P* wave velocities, seismicity, and gravity data, *Geochem. Geophys. Geosyst.*, *2*, doi:10.1029/2000GC000096.

Mazzotti, S., X. Le Pichon, P. Henry, and S.-I. Miyazaki (2000), Full interseismic locking of the Nankai and Japan-west Kurile subduction zones: An analysis of uniform elastic strain accumulation in Japan constrained by permanent GPS, *J. Geophys. Res.*, *105*, 13,159–13,177.

McCaffrey, R. (1997), Influences of recurrence times and fault zone temperatures on the age-rate dependence of subduction zone seismicity, *J. Geophys. Res.*, *102*, 22,839–22,854.

Miura, S., A. Nakanishi, N. Takahashi, S. Kodaira, T. Tsuru, A. Ito, R. Hino, and Y. Kaneda (2001), Seismic velocity structure of Japan trench off Miyagi forearc region, Northeastern Japan, using airgun-OBS data, *Eos Trans. AGU*, *82*(47), Abstract T22C-0937.

Miura, S., S. Kodaira, A. Nakanishi, T. Tsuru, M. Takahashi, N. Hirata, and Y. Kaneda (2003), Structural characteristics controlling the seismicity of southern Japan Trench fore-arc region, revealed by ocean bottom seismographic data, *Tectonophysics*, *323*, 79–102.

Moore, D. E., D. A. Lockner, M. Shengli, R. Summers, and J. D. Byerlee (1997), Strengths of serpentinite gouges at elevated temperatures, *J. Geophys. Res.*, *102*, 14,787–14,801.

Moore, G. F., and D. E. Karig (1980), Structural geology of Nias Island, Indonesia: Implications for subduction zone tectonics, *Am. J. Sci.*, *280*, 180–223.

Natawidjaja, D. H., K. Sieh, S. N. Ward, H. Cheng, R. L. Edwards, J. Galetzka, and B. W. Suwargadi (2004), Paleogeodetic records of seismic and aseismic subduction from central Sumatra microatolls, Indonesia, *J. Geophys. Res.*, *109*, B04306, doi:10.1029/2003JB002398.

Newcomb, K. R., and W. R. McCann (1987), Seismic history and seismotectonics of the Sunda Arc., *J. Geophys. Res.*, *92*, 421–439.
Oleskevich, D. A., R. D. Hyndman, and K. Wang (1999), The updip and downdip limit to great subduction earthquakes: Thermal and structural models of Cascadia, South Alaska, SW Japan and Chile, *J. Geophys. Res.*, *104*, 14,965–14,991.
Pacheco, J. F., L. R. Sykes, and C. H. Scholz (1993), Nature of seismic coupling along simple plate boundaries of the subduction type, *J. Geophys. Res.*, *98*, 14,133–14,159.
Peacock, S. M. (2000), Thermal structure and metamorphic evolution of subducting slabs, in *Inside the Subduction Factory*, *Geophys. Monogr. Ser.*, vol. 138, edited by J. Eiler, pp. 7–22, AGU, Washington, D. C.
Peacock, S. M., and R. D. Hyndman (1999), Hydrous minerals in the mantle wedge and the maximum depth of subduction thrust earthquakes, *Geophys. Res. Lett.*, *26*, 2517–2520.
Peacock, S. M., and K. Wang (1999), Seismic consequences of warm versus cool subduction metamorphism: Examples from southwest and northeast Japan, *Science*, *286*, 937–939.
Peltier, W. R., and A. M. Tushingham (1989), Global sea level rise and the green house effect, *Science*, *244*, 806–810.
Pollack, H., S. J. Hurter, and J. R. Johnson (1993), Heat flow from the Earth's interior: Analysis of the global data set, *Rev. Geophys.*, *31*(3), 267–280.
Prawirodirdjo, L., et al. (1997), Geodetic observations of interseismic strain segmentation at the Sumatra subduction zone, *Geophys. Res. Lett.*, *24*, 2601–2604.
Rivera, L., K. Sieh, D. Helmberger, and D. Natawidjaja (2002), A comparative study of the Sumatran subduction-zone earthquakes of 1935 and 1984, *Bull. Seismol. Soc. Am.*, *92*, 1721–1736.
Saltus, R. W., and R. J. Blakely (1995), HYPERMAG: An interactive, 2- and 2.5-dimensional gravity and magnetic modeling program, version 3.5, U.S. Geol. Surv., Reston, Va.
Samuel, M. A. (1994), The structural and stratigraphic evolution of islands at the active margin of the Sumatran forearc, Indonesia., Ph.D. thesis, Univ. of London, London.
Samuel, M. A., N. A. Harbury, M. E. Jones, and S. J. Matthews (1995), Inversion-controlled of an outer-arc ridge: Nias Island, offshore Sumatra, in *Basin Inversion*, edited by J. H. Buchanan and P. G. Buchanan, *Geol. Soc. Spec. Publ.*, *88*, 473–492.
Sandwell, D. T., and W. H. F. Smith (1997), Marine gravity anomaly from Geosat and ERS 1 satellite altimetry, *J. Geophys. Res.*, *102*, 10,039–10,054.
Savage, J. C. (1983), A dislocation model of strain accumulation and release at a subduction zone, *J. Geophys. Res.*, *88*, 4983–4996.
Scholz, C. H. (1998), Earthquakes and friction laws, *Nature*, *391*, 37–42.
Sieh, K., S. N. Ward, D. Natawidjaja, and B. W. Suwargadi (1999), Crustal deformation at the Sumatra subduction zone revealed by coral data, *Geophys. Res. Lett.*, *26*, 3141–3144.
Simoes, M. (2002), Croissance corallienne et mouvements verticaux le long de la zone de subduction a Sumatra: Implications sur l'extension de la zone sismogene en profondeur, DEA thesis, Ecole Normale Superieure, Paris.
Singh, S. J., and S. Rani (1993), Crustal deformation associated with two-dimensional thrust faulting, *J. Phys. Earth*, *41*, 87–101.
Takahashi, N., S. Kodaira, T. Tsuru, J. Park, Y. Kaneda, H. Kinoshita, S. Abe, M. Nishino, and R. Hino (2000), Detailed plate boundary structure off northeast Japan coast, *Geophys. Res. Lett.*, *27*, 1977–1980.
Taylor, F. W., J. Frohlich, J. Lecolle, and M. Strecker (1987), Analysis of partially emerged corals and reef terraces in the central Vanuatu arc: Comparison of contemporary coseismic and nonseismic with Quaternary vertical movements, *J. Geophys. Res.*, *92*, 4905–4933.
Tichelaar, B. W., and L. J. Ruff (1993), Depth of seismic coupling along subduction zones, *J. Geophys. Res.*, *98*, 2017–2037.
Turcotte, D. L., and G. Schubert (2002), *Geodynamics*, Cambridge Univ. Press, New York.
Vacquier, V., and P. T. Taylor (1966), Geothermal and magnetic survey off the coast of Sumatra. 1. Presentation of data, *Bull. Earthquake Res. Inst. Univ. Tokyo*, *44*, 531–540.
Vergne, J., R. Cattin, and J.-P. Avouac (2001), On the use of dislocations to model interseismic strain and stress build-up at intracontinental thrust faults, *Geophys. J. Int.*, *147*, 155–162.
Von Herzen, R., C. Ruppel, P. Molnar, M. Nettles, S. Nagihara, and G. Elkstrom (2001), A constraint on the shear stress at the Pacific-Australian plate boundary from heat flow and seismicity at the Kermadec forearc, *J. Geophys. Res.*, *106*, 6817–6833.
Wang, K., H. Dragert, and H. J. Melosh (1994), Finite element study of uplift and strain across Vancouver Island, *Can. J. Earth Sci.*, *31*, 1510–1522.
Wang, K., R. Wells, S. Mazzotti, R. D. Hyndman, and T. Sagiya (2003), A revised dislocation model of interseismic deformation of the Cascadia subduction zone, *J. Geophys. Res.*, *108*(B1), 2026, doi:10.1029/2001JB001227.
Wiens, D. A., and S. Stein (1983), Age dependence of oceanic intraplate seismicity and implications for lithosphere evolution, *J. Geophys. Res.*, *88*, 6455–6468.
Zachariasen, J., K. Sieh, F. W. Taylor, R. L. Edwards, and W. S. Hantoro (1999), Submergence and uplift associated with the giant 1833 Sumatran subduction earthquake, Evidence from coral microatolls, *J. Geophys. Res.*, *104*, 895–919.
Zachariasen, J., K. Sieh, F. W. Taylor, and W. S. Hantoro (2000), Modern vertical deformation above the Sumatran subduction zone: Paleogeodetic insights from coral microatolls, *Bull. Seismol. Soc. Am.*, *90*, 897–913.
Zienkiewicz, O. C., and R. L. Taylor (1989), *The Finite Element Method*, McGraw-Hill, New York.

J. P. Avouac and M. Simoes, Geology and Planetary Sciences Division, MC 170-25, California Institute of Technology, Pasadena, CA 91125, USA. (simoes@gps.caltech.edu)

R. Cattin, Laboratoire de Geologie, Ecole Normale Supérieure, 24, rue Lhomond. 75251 Paris Cedex 05, France.

P. Henry, College de France Chaire de Geodynamique, Europole de l'Arbois, BP 80, F-13545 Aix-en-Provence Cedex 04, France.